Exploring New Metal Electrodes for Ferroelectric Aluminum-Doped Hafnium Oxide

Hojoon Ryu, Kai Xu, Jinhong Kim, Sangmin Kang, Ji Guo, and Wenjuan Zhu, *Member, IEEE*

***Abstract*— In this paper, we explore new metal electrodes for ferroelectric capacitors based on Al-doped HfO_2. We find that Ti/Pd, Ti/Au, and W top electrodes can induce much higher remanent polarization as compared to the traditional TiN top electrode. The endurance of the capacitors with Ti/Pd electrodes is also much better than that with TiN and W electrodes. These results indicate that Ti/Pd is a very promising candidate for ferroelectric Al-doped HfO_2. In addition, we find that the remanent polarization reaches maximum when the annealing temperature is around 900 °C–950 °C. At a given annealing temperature, the optimal Hf-to-Al cycle ratio corresponding to the highest remanent polarization is around 23:1. With optimized process conditions, we demonstrate high-performance Ti/Pd gated ferroelectric Al-doped HfO_2 capacitors with remanent polarization up to 20 $\mu C/cm^2$, endurance higher than 10^8 cycles, and retention over ten years at room temperature. Another interesting feature of the ferroelectric capacitors with Ti/Pd electrodes is high tunability of polarization by external pulses, which will be important for neurosynaptic computing applications.**

***Index Terms*— Ferroelectric devices, ferroelectric films, ferroelectric materials.**

I. Introduction

DOPED HfO_2 has emerged as a new class of ferroelectric material in recent years. As compared to the traditional perovskite ferroelectric materials, HfO_2-based ferroelectrics have several advantages, including excellent scalability, high coercive field, and full compatibility with CMOS processes [1]–[4]. Several dopants have been reported to be able to induce ferroelectricity in HfO_2, including silicon (Si) [5], [6], aluminum (Al) [7], gadolinium (Gd) [8], yttrium (Y) [9], strontium (Sr) [10], barium (Ba) [11], and lanthanum (La) [2]. Among these dopants, aluminum has attracted significant research interest, because Al_2O_3 is a commonly used high-k dielectric and ALD Al_2O_3 tools are widely available in many industry and research institutes. It has been reported that Al-doped HfO_2 undergoes a phase transformation from the initial state (tetragonal, t-phase or monoclinic phase, and m-phase) to noncentrosymmetric orthorhombic phase (o-phase) upon applying an electric field or thermal annealing [12], [13]. In the ferroelectric phase transition, capping electrodes and bottom substrates play important roles [12], [14], [15]. It has been found that, with a TiN capping layer, the silicon-doped HfO_2 transformed into the orthorhombic ferroelectric phase after annealing, while without TiN capping layer confinement, a monoclinic/tetragonal phase mixture was formed [5]. Therefore, TiN electrodes were widely used in many research works related to ferroelectric HfO_2. Besides TiN, Pt electrodes on Zr-doped HfO_2 were reported to reduce the degradation of the polarization during forming gas annealing [16]. For Gd-doped HfO_2, it is found that TaN can enhance the stabilization of the ferroelectric phase as compared to TiN electrodes [17]. Ir, however, was found to lower the polarization as compared to TiN [18]. For Al-doped HfO_2, to the best of our knowledge only TiN electrode has been investigated so far, and remanent polarization is in the range of 5 to 15 $\mu C/cm^2$ for planar device structure [3], [7], [19]–[21]. To further enhance the ferroelectricity, a systematic study to explore new metal electrodes is needed. In this paper, we investigated ferroelectric capacitors based on Al-doped HfO_2 with various metal electrodes including Ti/Pd, Ti/Au, W, and TiN. Based on these metal electrodes, we studied the impact of Al composition, annealing temperatures, and substrate on the ferroelectricity, leakage current, endurance, and retention of the ferroelectric capacitors.

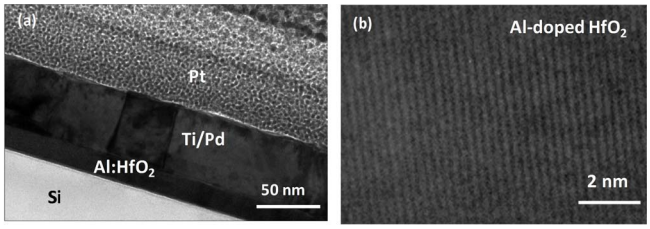

Fig. 1. (a) Cross-sectional TEM image of the Al-doped HfO_2 capacitor with Ti/Pd electrode on Si substrate annealed at 950 °C. (b) A close-up of the cross-sectional TEM image clearly showing that the Al-doped HfO_2 layer is crystallized.

II. Experiments

Planar metal–insulator–semiconductor (MIS) capacitors were fabricated on highly doped (100) p-type Si substrates.

Manuscript received February 20, 2019; revised March 19, 2019; accepted March 20, 2019. Date of publication April 10, 2019; date of current version April 22, 2019. This work was supported in part by the National Science Foundation (NSF) under Grant ECCS 16-53241 CAR and in part by the Office of Naval Research (ONR) under Grant NAVY N00014-17-1-2973. The review of this paper was arranged by Editor C. Monzio Compagnoni. *(Corresponding author: Wenjuan Zhu.)*

The authors are with the Department of Electrical and Computer Engineering, University of Illinois at Urbana–Champaign, Urbana, IL 61801 USA (e-mail: hojoonr2@illinois.edu; kaixu86@illinois.edu; jkim686@illinois.edu; smkang@illinois.edu; gj.xjtu@hotmail.com; wjzhu@illinois.edu).

Color versions of one or more of the figures in this paper are available online at http://ieeexplore.ieee.org.

Digital Object Identifier 10.1109/TED.2019.2907070

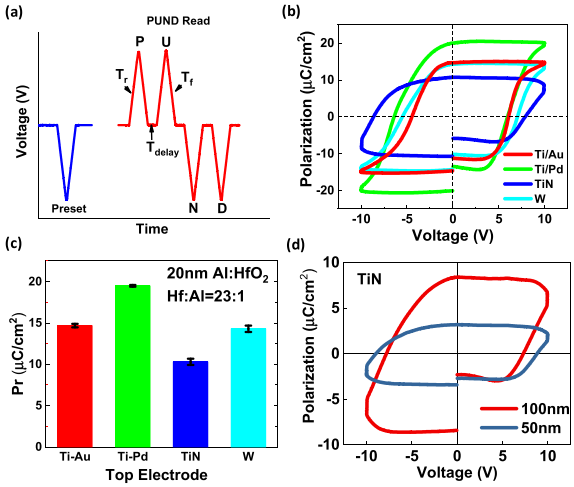

Fig. 2. (a) Illustration of pulse sequence in the PUND measurement. The amplitudes of the preset and the PUND pulses are 10 V. The pulse width is 0.1 μs. The rise time (t_r), fall time (t_f), and delay time between pulses (t_{delay}) are 1 μs. The preset pulse and the PUND pulses are in two separate test programs. The wait time between the preset and the PUND pulses is typically a couple of seconds. (b) P–V loops of Al-doped HfO_2 capacitors with various top electrodes (Ti/Pd, Ti/Au, W, and TiN). The thicknesses of Ti/Pd, Ti/Au, and W electrodes are 40–50 nm, while the thickness of TiN is 100 nm. (c) Statistics of the remanent polarization of the Al-doped HfO_2 capacitors with various top electrodes. For each wafer, we measured three to five capacitors. (d) Polarization as a function voltage for Al-doped HfO_2 with 100 and 50 nm TiN.

The resistivity of the silicon wafer is 0.001–0.005 Ω·cm. Al-doped HfO_2 films of 20 nm thickness were deposited using a Cambridge Nanotech Atomic Layer Deposition (ALD) system at a 200 °C substrate temperature. The Al concentration in the film was varied by tuning the cycle ratio between the Hf precursor [tetrakis (ethylmethylamino) hafnium (TEMAH)] and Al precursor [trimethylaluminium (TMA)]. The Ti/Pd and Ti/Au electrodes were deposited by Temescal E-beam evaporator, while TiN and W electrodes were deposited by Lesker dual-gun sputtering system and AJA Orion 3 sputter tool, respectively. The encapsulated HfO_2 films were then annealed in a rapid thermal annealing (RTA) system. The annealing was performed for 1–2 s at various temperatures from 800 °C to 1000 °C. The N_2 atmosphere was used for the RTA process. The capacitor area is 45 μm × 45 μm. Fig. 1(a) shows a cross-sectional TEM image of Al-doped HfO_2 with Ti/Pd top electrode on silicon substrate annealed at 950 °C. The close-up TEM image of the Al-doped HfO_2 layer in Fig. 1(b) shows that the doped HfO_2 film is crystallized after annealing.

III. Results and Discussion

A. Impact of Top Electrodes on the Ferroelectricity of Al-Doped HfO_2

We explored various metal materials as the top electrodes including Ti/Pd, Ti/Au, W, and TiN. The polarization of the capacitors was measured using the positive-up-negative-down (PUND) method [22]. Fig. 2(a) illustrates the waveform of the PUND measurement. The polarization versus voltage (P–V) loops for Al-doped HfO_2 capacitors with these electrodes are shown in Fig. 2(b), and the statistics of remanent polarization, P_r, are shown in Fig. 2(c). Among these four electrodes, the Ti/Pd electrode gives the highest remanent polarization value in the ferroelectric capacitors. At 10 V, the remanent polarization in Al-doped HfO_2 capacitor with Ti/Pd electrode can reach 20 $\mu C/cm^2$. We speculate that the internal strain induced by Ti/Pd favors the formation of ferroelectric phase in Al-doped HfO_2. Note that in the PUND measurement, the preset and PUND read pulses are located in two separate test programs. It typically takes a few seconds for the parameter analyzer to close the preset test program and start the PUND test program. This time delay between the preset pulse and the PUND pulses is one of the main causes of the gaps between the start and end part of the hysteresis loops. The displacement of the polarization hysteresis loop along the electric field axis may originate from the asymmetric structure of the MIS capacitor, the nonswitching layer between the ferroelectric layer and the silicon substrate, and/or interface trapped charges at the silicon interfaces [23]–[27]. The coercive voltages in the capacitors with TiN electrodes are higher than that with Ti/Au, Ti/Pd and W, which is probably due to the high resistivity of the TiN film. For the capacitors shown in Fig. 2(a), the thicknesses of the Ti/Pd, Ti/Au, and W electrodes are 40–50 nm, while the thickness of TiN is 100 nm. The process condition of TiN is based on the previous report [21]. In order to evaluate the impact of the TiN thickness on the remanent polarization, we fabricated the Al-doped HfO_2 capacitors with two different TiN thicknesses. Fig. 2(d) shows the P–V loop measured on the capacitors with 50 and 100 nm TiN. The capacitor with 100 nm TiN shows much higher remanent polarization than that with the 50 nm TiN. These results indicate that if the electrode thicknesses are comparable, the remanent polarization in capacitors with Ti/Pd will be even larger than that with TiN.

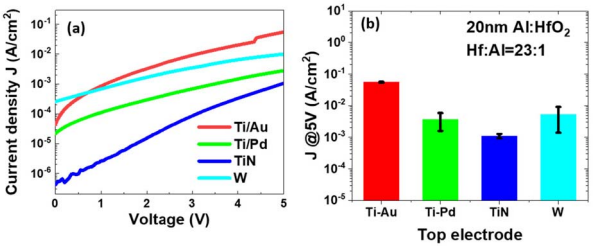

Fig. 3. (a) Leakage current density as a function of gate voltage and (b) statistics of the leakage current density at 5 V of Al-doped HfO_2 capacitors with various top electrodes. For each wafer, we measured three to five capacitors.

In addition to the remanent polarization, the leakage current density is also impacted by the top electrodes. As shown in Fig. 3(a) and (b), the leakage current density for capacitors with Ti/Pd electrode is much lower than that with Ti/Au electrode and is comparable to that with W electrode. This result can be attributed to the fact that different metals have different resistivity, thermal stability, work function, mechanical strain, surface roughness, and density of interface states at the metal/ferroelectric interface, which can lead to different leakage current density. In particular, the resistivity

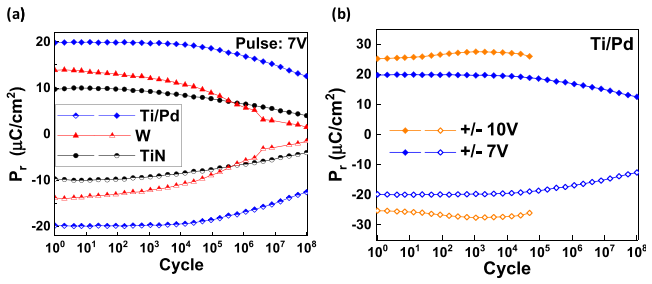

Fig. 4. (a) Endurance of Al-doped HfO_2 capacitors with various top electrodes. The amplitude of the cycling pulses is 7 V and the amplitude of the PUND read pulses is 10 V. (b) Endurance of Al-doped HfO_2 capacitors with Ti/Pd electrode measured at two different cycling voltages: ±7 and ±10 V. The amplitudes of the PUND read pulses in both tests are 10 V. The timings for both cycling pulses and PUND pulses are the same. The pulse width is 100 ns. The rise/fall time is 1 μs and the delay between two pulses is 1 μs.

of these TiN films is higher than that of the other three metal electrodes, which can result in lower leakage current in TiN capacitors. The thermal stability of Au is worse than the other three electrodes, which can lead to higher leakage current in Au capacitors. Here we limited our dc IV measurements to 5 V, since we noticed that the devices are more prone to break down when the voltage is in dc mode instead of short pules. This trend was also observed in $BiFeO_3$, which was attributed to the local joule heating under dc bias [28]. It is worth mentioning that PUND measurement is effective to eliminate the influence of the leakage current on the extraction of polarization charges [29], [30]. In PUND measurement, the polarization is extracted from the subtraction of the charges collected from two consecutive pulses, the contribution from the nonferroelectric polarization and the leakage current are eliminated. Therefore, for ultrathin ferroelectric film with high leakage current, the PUND measurement is more accurate than direct hysteresis measurement with single triangular voltage pulse. Note that the leakage current density of these samples is higher than that reported in [7], [20], and [21].

Considering both remanent polarization and leakage current density, Ti/Pd is the most promising electrode among these metals. To the best of our knowledge, this is the first report of Ti/Pd as a gate electrode for ferroelectric HfO_2.

The metal materials in the top electrode can also impact the endurance of the ferroelectric capacitors. Fig. 4(a) shows the endurance of the capacitors with various top electrode materials (TiN, Ti/Pd, and W). The amplitude of the cycling pulses is 7 V and the amplitude of the PUND read pulses is 10 V. The endurance of the capacitors with Ti/Pd is much better than that with TiN and W electrodes. After 10^8 cycles, 63.5% of initial polarization is maintained for the Ti/Pd capacitor, 41.1% of initial polarization is left for the TiN capacitor, while only 10.9% is left for the W capacitor. The endurance characteristics also depend on the operating voltage, as depicted in Fig. 4(b). At the ±7 V cycling voltage (3.5 MV/cm at 20 nm), the ferroelectric Al-doped HfO_2 shows the characteristic fatigue behavior of ferroelectric materials, while at ±10 V cycling voltage, hard breakdown becomes the limiting factor for the endurance.

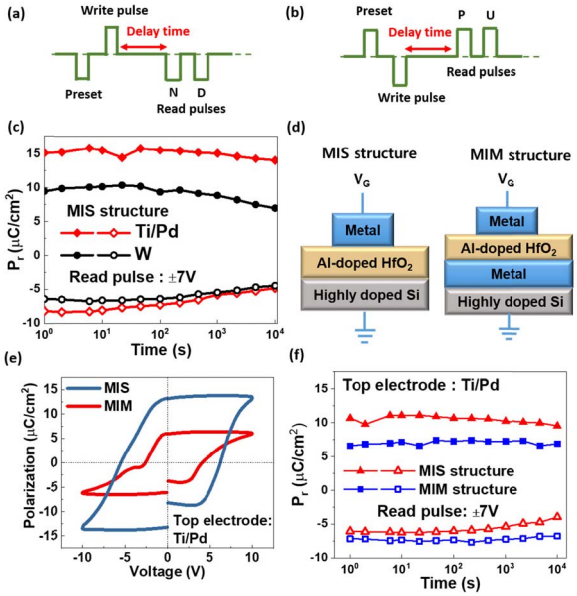

Fig. 5. Retention of Al-doped HfO_2. (a) and (b) Illustrations of the waveforms of the retention tests with positive and negative write pulses, respectively. The amplitudes of both the write pulses and the read pulses are 7 V. (c) Retention of MIS Al-doped HfO_2 capacitors with Ti/Pd and W top electrodes. (d) Illustrations of an MIS and an MIM capacitor with ferroelectric HfO_2. (e) P–V loops of an MIM and MIS capacitor. The top electrodes for both MIM and MIS capacitors are Ti/Pd. The bottom electrode for the MIM capacitor is TiN. The substrate for the MIS capacitor is silicon. (f) Retention of MIS and MIM Al-doped HfO_2 capacitors with Ti/Pd top electrodes. The retention is tested at room temperature.

Similar to endurance, the retention of the ferroelectric capacitors also depends on the top electrodes. The waveforms of the retention tests are illustrated in Fig. 5(a) and (b). Each test consists of a preset, a write and two read pulses. The amplitudes of both the write pulses and the read pulses are 7 V. The retention of MIS capacitors with Ti/Pd and W electrodes is shown in Fig. 5(c). We can see that the retention of the capacitors with Ti/Pd is much longer than that with W. After 10^4 second, 81% polarization remains for the Ti/Pd capacitor while only 72% remains for the W capacitor. For these capacitors, the substrate is highly doped silicon. Due to the incomplete charge compensation at the silicon interface, a depolarization field can be formed, which degrades the retention of the polarization in HfO_2. To further improve the retention time, metal-insulator-metal (MIM) capacitors were also fabricated. Fig. 5(d) illustrates the MIS and MIM structures. For MIM capacitors, the TiN film was deposited on Si substrate by sputtering. The thickness of the bottom TiN is 12 nm. Fig. 5(e) shows the P–V loops measured on MIS and MIM capacitors. The remanent polarization of the MIS structure is higher than that of the MIM structure. We suspect that the low remanent polarization of the MIM capacitor is due to the surface roughness of the bottom TiN. Fig. 5(f) shows the retention of the MIM capacitor and MIS capacitor with the same top electrode Ti/Pd. We can see that the retention of the MIM capacitor is much better than that of the MIS capacitor. For the MIM capacitor, 98.5% polarization remains after 10^4 s, and it can be extrapolated that over 90% polarization remains after ten years.

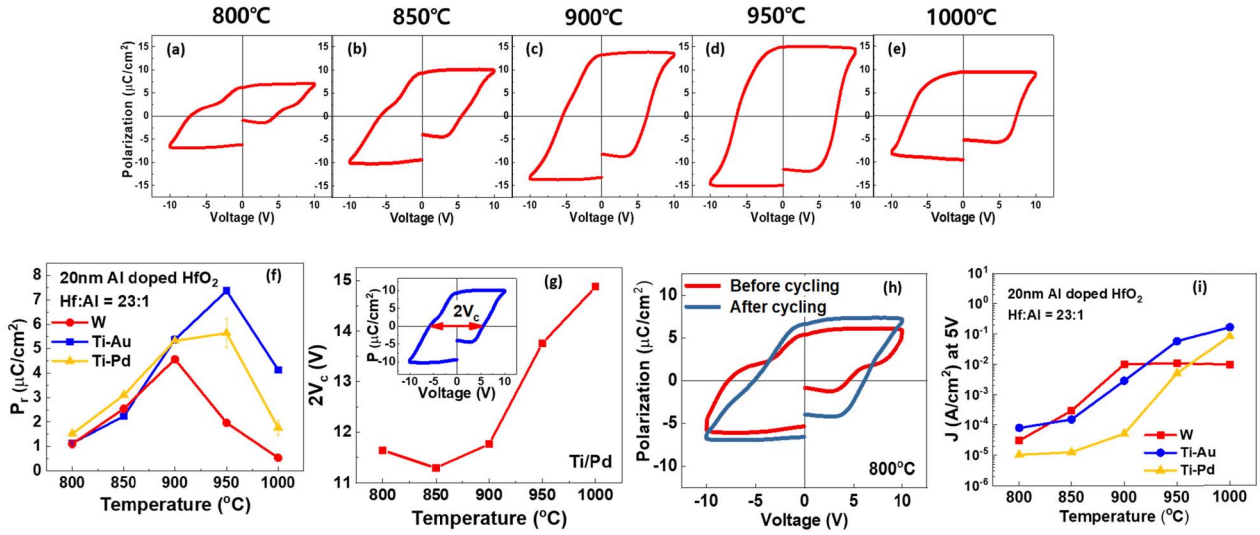

Fig. 6. Impact of annealing temperature on the properties of the Al-doped HfO_2 film. (a)–(e) P–V loops of Al-doped HfO_2 annealed at various temperatures from 800 °C to 1000 °C. The top electrodes are Ti/Pd. The amplitude of the PUND read pulses is 10 V. (f) Remnant polarization as a function of annealing temperature for Al-doped HfO_2 capacitors with Ti/Pd, Ti/Au and W electrodes. The amplitude of the PUND read pulses is 7 V. (g) 2 V_c as a function of annealing temperature for Al-doped HfO_2 capacitors with Ti/Pd electrode. The inset illustrates the definition of 2 V_c: the difference between positive and negative coercive voltage in the P–V loop. (h) P–V loops of Al-doped HfO_2 annealed at 800 °C before and after cycling 10^4 pulses. The amplitude of the cycling pulses is 10 V. (i) Leakage current density at 5 V as a function of annealing temperature of the Al-doped HfO_2 capacitor with various electrodes.

B. Impact of Annealing Condition and Composition Ratio on the Ferroelectricity of Al-Doped HfO_2

In addition to electrodes, annealing temperature also can affect the ferroelectricity significantly. The P–V loops of Al-doped HfO_2 annealed at various temperatures are shown in Fig. 6(a)–(e). As the annealing temperature increases, the pinched hysteresis loop disappears and the remanent polarization increases, indicating that a larger portion of the film is transforming to ferroelectric phase. Fig. 6(f) shows the $2P_r$ as a function of annealing temperature for Al-doped HfO_2 with various top electrodes. We can see that the $2P_r$ value reaches its maximum around 900 °C – 950 °C. When temperature is above 950 °C, the $2P_r$ value starts to decrease with increasing temperature. The decrement of remanent polarization at high temperatures may be due to the formation of interfacial silicon oxide between silicon substrate and HfO_2 layer, or the formation of non-ferroelectric phase, such as monoclinic phase in the Al-doped HfO_2 layer. This nonferroelectric layer (also known as a "dead layer") will reduce the effective electric field dropped on the ferroelectric HfO_2, which will decrease the measured polarization at a given gate voltage [17], [22], [23]. In addition, this nonferroelectric layer will induce a depolarization field, which may reduce the retention time of the ferroelectric devices. Therefore, annealing the film at an optimal temperature is critical for the device performance and reliability. The coercive field of the ferroelectric HfO_2 is also influenced by the annealing temperature. Here, we define the difference between positive and negative coercive voltage as $2V_c$, illustrated in the inset of Fig. 6(g). The $2V_c$ as a function of annealing temperature is shown in Fig. 6(g). When the temperature is above 900 °C, 2 V_c increases monotonically with increasing annealing temperature. This increment of coercive voltage is due to the formation of non-ferroelectric layer and the increasing voltage drop on the nonferroelectric layer. Note, for the capacitors annealing at low temperature (800 °C), there is a kink in the P–V loop, shown in Fig. 6(a). We found that after cycling 10^4 pulses, the kink disappeared and the $2P_r$ value increased slightly, shown in Fig. 6(h). This behavior was also observed in PZT samples, where the constricted hysteresis was attributed to the domains with different internal bias fields [26]. The field cycling can either cause the redistribution of the dopant ions or neutralization of the inhomogeneously distributed centers by the space charges, which leads to a relaxed, open hysteresis [26], [31].

The annealing temperature can also impact the leakage current, as shown in Fig. 6(i). When the annealing temperature is below 900 °C, the leakage current increases dramatically with increasing temperature. This is because, as the temperature increases, a larger portion of the amorphous HfO_2 film crystallizes into poly-crystalline film. As a result, the leakage current related to the grain boundaries increases with temperature [32]. When the annealing temperature is above 900 °C, the leakage current increment slows down. This is consistent with previous observation of the interfacial layer growth in the HfO_2/Si capacitors when they were annealed at high temperatures [32].

In addition to the annealing temperature, the Hf-to-Al ratio is also a critical parameter in determining the ferroelectricity of the film. We varied the Al concentration in the HfO_2 by tuning the cycle ratio between the Hf precursor and Al precursor. Fig. 7 shows the remanent polarization of the capacitors as a function of the cycle ratio between Hf and Al. Regardless of the top electrode material we used, all devices show nonmonotonic dependence of the remanent polarization on the cycle ratio, and an optimal Hf-to-Al ratio is in the range of 21:1 to 25:1.

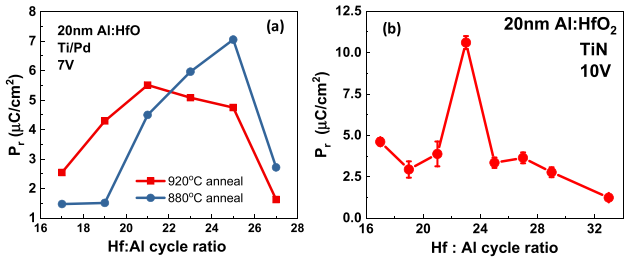

Fig. 7. Remanent polarization as a function of Hf-to-Al cycle ratio for 20-nm Al-doped HfO_2 capacitors with (a) Ti/Pd electrodes and (b) TiN electrodes. The amplitude of the PUND read pulse is 7 V for the Ti/Pd capacitors, while it is 10 V for the TiN capacitors.

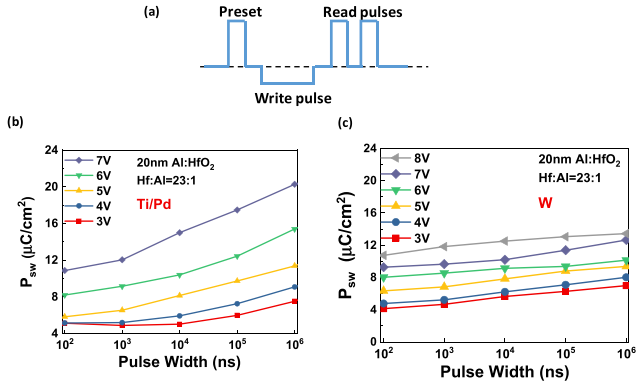

Fig. 8. (a) Illustration of the pulse sequence for variable write polarization measurement. (b) Switching polarization (P_{sw}) as a function of pulse width at various pulse voltages for 20-nm Al-doped HfO_2 with Ti/Pd electrode on silicon substrate. (c) Switching polarization (P_{sw}) as a function of pulse width at various pulse voltages for 20-nm Al-doped HfO_2 with W electrode on silicon substrate.

C. Switching Dynamics of Al-Doped HfO_2-Based Devices

The polarization in ferroelectric HfO_2 is not only determined by the process conditions but also tunable by the operating conditions. We carried out the variable-write measurement on the Al-doped HfO_2 with Ti/Pd and W electrodes. Fig. 8(a) illustrates the pulse sequence for variable write measurement. Following a positive preset pulse, a variable negative write pulse was applied to the capacitor. The charge switched by the variable write pulse was then evaluated by the comparison of two consecutive positive sensing pulses, recording the polarization reversal and the linear contribution of the capacitor. Fig. 8(b) shows the measured switching polarization as a function of write pulse width with various pulse amplitudes for 20-nm Al-doped HfO_2 with Ti/Pd electrode. A steep increase in switching polarization can be observed for high voltages, whereas for pulses with low amplitude, only slow polarization reversal occurs. The general trend toward higher switching speeds with increasing voltage shows that polarization reversal is a statistical process strongly accelerated when exceeding certain activation fields. This result also indicates that the amount of ferroelectric polarization can be continuously tuned by external pulses, which will be very important for ferroelectric synapsis applications. Note that the capacitor with Ti/Pd electrode shows higher remanent polarization and greater tunability than that with W electrode, shown in Fig. 8(c). The result indicates that the Ti/Pd capacitor with wider design window is more promising for neurosynaptic computing applications as compared to the W electrode.

IV. Conclusion

In summary, we explored three new metal materials as top electrodes for Al-doped HfO_2: Ti/Pd, Ti/Au, and W. First, we found that the ferroelectric Al-doped HfO_2 capacitors with Ti/Pd electrodes have much higher remanent polarization and better endurance as compared to those with TiN, W, and Ti/Au electrodes. The retention of the capacitors with Ti/Pd electrode is also longer than that with W electrode. These results indicate that Ti/Pd is a very promising electrode candidate for ferroelectric Al-doped HfO_2. The remanent polarization reaches maximum around 900 °C – 950 °C. When the annealing temperature is above 950 °C, the remanent polarization starts to decrease and the coercive field starts to increase due to the formation of nonferroelectric layer. Third, we found that the optimal Hf-to-Al cycle ratio is around 23:1, regardless the metal electrode material. Based on the optimized process conditions, we demonstrated high-performance ferroelectric Al-doped HfO_2 with remanent polarization up to 20 $\mu C/cm^2$ at 10 V and endurance higher than 10^8 cycles. For the MIM capacitor based on Al-doped HfO_2, we can extrapolate that more than 90% of the original polarization will remain after 10 years. This study demonstrated the feasibility of high-performance ferroelectric Al-doped HfO_2. We envision that ferroelectric Al-doped HfO_2 will have broad applications in ferroelectric random access memories, ferroelectric tunneling junctions, and piezoelectric devices.

References

[1] E. Yurchuk *et al.*, "Impact of scaling on the performance of HfO_2-based ferroelectric field effect transistors," *IEEE Trans. Electron Devices*, vol. 61, no. 11, pp. 3699–3706, Nov. 2014. doi: 10.1109/Ted.2014.2354833.

[2] J. Muller *et al.*, "Ferroelectric hafnium oxide: A CMOS-compatible and highly scalable approach to future ferroelectric memories," in *IEDM Tech. Dig.*, Dec. 2013, pp. 1081–1084. doi: 10.1109/IEDM.2013.6724605.

[3] U. Schroeder *et al.*, "Hafnium oxide based CMOS compatible ferroelectric materials," *ECS J. Solid State Sci. Technol.*, vol. 2, no. 4, pp. N69–N72, 2013. doi: 10.1149/2.010304jss.

[4] A. Chernikova *et al.*, "Ultrathin $Hf_{0.5}Zr_{0.5}O_2$ ferroelectric films on Si," *ACS Appl. Mater. Interfaces*, vol. 8, no. 11, pp. 7232–7237, Mar. 2016. doi: 10.1021/acsami.5b11653.

[5] T. S. Böscke *et al.*, "Phase transitions in ferroelectric silicon doped hafnium oxide," *Appl. Phys. Lett.*, vol. 99, no. 11, 2011, Art. no. 112904. doi : 10.1063/1.3636434.

[6] P. D. Lomenzo, Q. Takmeel, S. Moghaddam, and T. Nishida, "Annealing behavior of ferroelectric Si-doped Hf_{O2} thin films," *Thin Solid Films*, vol. 615, pp. 139–144, Sep. 2016. doi: 10.1016/j.tsf.2016.07.009.

[7] S. Mueller *et al.*, "Incipient ferroelectricity in Al-doped HfO_2 thin films," *Adv. Funct. Mater.*, vol. 22, no. 11, pp. 2412–2417, 2012. doi: 10.1002/adfm.201103119.

[8] S. Mueller, C. Adelmann, A. Singh, S. Van Elshocht, U. Schroeder, and T. Mikolajick, "Ferroelectricity in gd-doped HfO_2 thin films," *ECS J. Solid State Sci. Technol.*, vol. 1, no. 6, pp. N123–N126, 2012. doi: 10.1149/2.002301jss.

[9] J. Müller *et al.*, "Ferroelectricity in yttrium-doped hafnium oxide," *J. Appl. Phys.*, vol. 110, no. 11, 2011, Art. no. 114113. doi: 10.1063/1.3667205.

[10] T. Schenk *et al.*, "Strontium doped hafnium oxide thin films: Wide process window for ferroelectric memories," in *Proc. Proc. Eur. Solid-State Device Res. Conf. (ESSDERC)*, Sep. 2013, pp. 260–263. doi: 10.1109/ESSDERC.2013.6818868.

[11] S. Starschich and U. Boettger, "An extensive study of the influence of dopants on the ferroelectric properties of Hf_{O2}," *J. Materials Chem. C*, vol. 5, no. 2, pp. 333–338, 2017. doi: 10.1039/C6TC04807B.

[12] T. S. Böscke, J. Müller D. Bräuhaus, U.Schröder, and U. Böttger, "Ferroelectricity in hafnium oxide thin films ," *Appl. Phys. Lett.*, vol. 99, no. 10, 2011, Art. no. 102903. doi: 10.1063/1.3634052.

[13] J. Müller *et al.*, "Ferroelectricity in HfO_2enables nonvolatile data storage in 28 nm HKMG," in *Proc. Symp. VLSI Technol. (VLSIT)*, Jun. 2012, pp. 25–26. doi: 10.1109/VLSIT.2012.6242443.

[14] S. W. Lee *et al.*, "Influences of metal, non-metal precursors, and substrates on atomic layer deposition processes for the growth of selected functional electronic materials," *Coordination Chem. Rev.*, vol. 257, nos. 23–24, pp. 3154–3176, 2013. doi: 10.1016/j.ccr.2013.04.010.

[15] S. J. Song *et al.*, "Substrate dependent growth behaviors of plasma-enhanced atomic layer deposited nickel oxide films for resistive switching application," *Chem. Mater.*, vol. 24, no. 24, pp. 4675–4685, 2012. doi: 10.1021/cm302182s.

[16] M. H. Park, H. J. Kim, Y. J. Kim, W. Lee, H. K. Kim, and C. S. Hwang, "Effect of forming gas annealing on the ferroelectric properties of $Hf_{0.5}Zr_{0.5}O_2$ thin films with and without Pt electrodes," *Appl. Phys. Lett.*, vol. 102, no. 11, 2013, Art. no. 112914, doi: 10.1063/1.4798265.

[17] M. Hoffmann *et al.*, "Stabilizing the ferroelectric phase in doped hafnium oxide," *J. Appl. Phys.*, vol. 118, no. 7, 2015, Art. no. 072006. doi: 10.1063/1.4927805.

[18] P. D. Lomenzo *et al.*, "Ferroelectric phenomena in Si-doped HfO_2 thin films with TiN and Ir electrodes," *J. Vac. Sci. Technol. B, Microelectron.*, vol. 32, no. 3, 2014, Art. no. 03D123. doi: 10.1116/1.4873323.

[19] P. Polakowski *et al.*, "Ferroelectric deep trench capacitors based on Al: HfO_2 for 3D nonvolatile memory applications," in *Proc. IEEE 6th Int. Memory Workshop (IMW)*, May 2014, pp. 1–4. doi: 10.1109/IMW.2014.6849367.

[20] K. Florent *et al.*, "Reliability study of ferroelectric Al: HfO_2 thin films for DRAM and NAND applications," *IEEE Trans. Electron Devices*, vol. 64, no. 10, pp. 4091–4098, Oct. 2017. doi: 10.1109/Ted.2017.2742549.

[21] N. Gong, X. Sun, H. Jiang, Q. Xia, and T. P. Ma, "Ferroelectricity of Al-doped HfO_2: Fast polarization switching, long retention and robust endurance," in *Proc. 46th IEEE Semiconductor Interface Spec. Conf.*, Arlington, VA, USA, Sep. 2015, p. 14.3.

[22] J. F. Scott, C. A. Araujo, H. B. Meadows, L. D. McMillan, and A. Shawabkeh, "Radiation effects on ferroelectric thin-film memories: Retention failure mechanisms," *J. Appl. Phys.*, vol. 66, no. 3, pp. 1444–1453, 1989. doi: 10.1063/1.344419.

[23] J. Scott, *Ferroelectric Memories*. Berlin, Germany: Springer, 2000.

[24] D. Dimos, W. L. Warren, M. B. Sinclair, B. A. Tuttle, and R. W. Schwartz, "Photoinduced hysteresis changes and optical storage in $(Pb,La)(Zr,Ti)_{O3}$ thin films and ceramics," *J. Appl. Phys.*, vol. 76, no. 7, pp. 4305–4315, 1994. doi: 10.1063/1.357316.

[25] G. Le Rhun, R. Bouregba, and G. Poullain, "Polarization loop deformations of an oxygen deficient $Pb(Zr0.25,Ti0.75)_{O3}$ ferroelectric thin film," *J. Appl. Phys.*, vol. 96, no. 10, pp. 5712–5721, 2004. doi: 10.1063/1.1789635.

[26] K. Carl and K. Hardtl, "Electrical after-effects in $Pb(Ti, Zr)_{O3}$ ceramics," *Ferroelectrics*, vol. 17, no. 1, pp. 473–486, 1977. doi: 10.1080/00150197808236770.

[27] M. Grossmann, O. Lohse, D. Bolten, U. Boettger, T. Schneller, and R. Waser, "The interface screening model as origin of imprint in $PbZr_xTi1\text{-}_xO_3$ thin films. I. Dopant, illumination, and bias dependence," *J. Appl. Phys.*, vol. 92, no. 5, pp. 2680–2687, Sep. 2002. doi: 10.1063/1.1498966.

[28] C. Wang *et al.*, "Switchable diode effect and ferroelectric resistive switching in epitaxial $BiFeO_3$ thin films," *Appl. Phys. Lett.*, vol. 98, no. 19, May 2011, Art. no. 192901. doi: 10.1063/1.3589814.

[29] S. Matsuo, T. Yamada, T. Kamo, H. Funakubo, M. Yoshino, and T. Nagasaki, "Indirect measurements of electrocaloric effect in ferroelectric thin films by positive-up-negative-down method," *J. Ceram. Soc. Jpn.*, vol. 125, no. 6, pp. 441–444, 2017. doi: 10.2109/jcersj2.16283.

[30] H. Naganuma, Y. Inoue, and S. Okamura, "Evaluation of electrical properties of leaky $BiFeO_3$ films in high electric field region by high-speed positive-up-negative-down measurement," *Appl. Phys. Rev.*, vol. 1, no. 6, 2008, Art. no. 061601. doi: 10.1143/apex.1.061601.

[31] T. Schenk *et al.*, "About the deformation of ferroelectric hystereses," *Appl. Phys. Rev.*, vol. 1, no. 4, Dec. 2014, Art. no. 041103. doi: 10.1063/1.4902396.

[32] W. J. Zhu, T. Tamagawa, M. Gibson, T. Furukawa, and T. P. Ma, "Effect of Al inclusion in HfO_2 on the physical and electrical properties of the dielectrics," *IEEE Electron Device Lett.*, vol. 23, no. 11, pp. 649–651, Nov. 2002. doi: 10.1109/Led.2002.805000.